

## Nonclassical Photon Statistics in Single-Molecule Fluorescence at Room Temperature

L. Fleury, J.-M. Segura, G. Zumofen, B. Hecht,\* and U. P. Wild

*Physical Chemistry Laboratory, Swiss Federal Institute of Technology, ETH-Z, CH-8092 Zürich, Switzerland*

(Received 24 June 1999)

The fluorescence of single terrylene molecules in a crystalline host is investigated at room temperature by scanning confocal optical microscopy. Photon arrival times are analyzed in terms of interphoton time distributions, second order correlation functions, and the variance of the photon number probability distribution. Antibunching at short times and bunching behavior for longer times is observed, associated with sub- and super-Poissonian statistics, respectively. A rate-equation analysis of the molecular level populations indicates an accelerated reverse intersystem crossing.

PACS numbers: 42.50.Dv, 32.50.+d, 33.80.-b, 61.16.Ch

Optical experiments with single quantum systems have contributed significantly to the basic understanding of light-matter interactions. Complementary to resonance fluorescence experiments with atoms in beams [1] and single ions in electromagnetic traps [2], single molecules embedded in solids at low temperature [3] have been used to study quantum optical effects such as photon antibunching [4], light shift [5], hyper-Raman and subharmonic resonances [6], and Rabi resonances [7]. Recent advances in fluorescence microscopy have allowed for the detection, imaging, and spectroscopy of single molecules also at room temperature [8]. Yet, room temperature experiments that reveal the nonclassical character of the fluorescence light emitted by a single molecule are very rare and, until now, could solely be performed by averaging the effects of a large number of single absorbers [9–11]. The reason for this is the limited amount of fluorescence photons available from a single molecule before photochemical destruction. Single dopant molecules in a solid matrix are potential candidates for numerous experiments where the presence of a single quantum system at a well defined location in space is essential [12,13]. It has been shown recently that the problem of rapid photo bleaching at room temperature can be overcome for terrylene molecules embedded in a crystal of *p*-terphenyl [14]. Here, photochemistry is drastically reduced because terrylene is efficiently protected by the host crystal. In this Letter we report on the fluorescence photon statistics of single terrylene molecules in a *p*-terphenyl crystal and demonstrate that quantum effects can be investigated using a desktop-scale apparatus at ambient conditions.

Crystal flakes of *p*-terphenyl with a thickness of  $\approx 3 \mu\text{m}$  doped with a low concentration of terrylene were grown by cosublimation according to standard procedures [15]. A scanning confocal optical microscope was employed to image single molecules of terrylene in *p*-terphenyl [14]. Terrylene was excited nonresonantly by a cw-Ar<sup>+</sup> laser at a wavelength of 514 nm and a typical excitation intensity of 500 kW/cm<sup>2</sup>. The excitation light was passed through a single mode fiber for spatial filtering. It was collimated, reflected by a dichroic mirror, and then focused

to a diffraction-limited spot by an oil-immersion objective (Leica, 1.3 NA,  $\infty$ ). The same objective collected the fluorescence, which was directed to a 50/50 nonpolarizing beam splitter after passing the dichroic mirror. A notch and a cutoff filter removed the residual back-reflected excitation light. The resulting two collimated fluorescence photon beams were focused onto the active areas of two single photon counting avalanche photodiodes (SPAD) of the same type.

Single-molecule fluorescence images were recorded by raster scanning the crystal through the focus by means of a linearized *x-y-z* piezo scan table and recording the number of counts for each pixel in a computer. In order to study the photon statistics of selected terrylene molecules, the sample scanner was moved to a position where a well isolated fluorescence spot occurred in the fluorescence image. The output pulses of the two SPADs were then fed into separate inputs of a two channel time interval analyzer (TIA) [16]. An electronic delay was imposed on one channel in order to minimize the effect of noise generated by the TIA at very short interphoton times. The dead time occurring in a single TIA channel is dominated by the dead time  $t_{\text{dead}} \approx 30 \text{ ns}$  of the SPAD. Photons arriving in different channels, however, can be recorded virtually free of dead time. In a typical experiment, the TIA acquires  $2 \times 10^6$  data points during  $\approx 20 \text{ s}$  indicating the arrival times with an accuracy of 0.5 ns as well as the acquisition channel for each detected photon. The molecules were in general stable enough to record several data sets at different excitation intensities before photobleaching.

A powerful method of data analysis is to calculate the second order correlation function [17,18]

$$g^{(2)}(\tau) = \langle I(t)I(t + \tau) \rangle / \bar{I}^2, \quad (1)$$

where  $I(t)$  is the photon rate at time  $t$  and  $\bar{I} = \langle I \rangle$ . In standard single-molecule experiments, different experimental techniques have been applied to obtain  $g^{(2)}$ . In the limit of short interphoton times ( $\approx 100 \text{ ns}$ ) start-stop methods are widely used [2,4]. The resulting histograms of interphoton times follow  $g^{(2)}$  for short enough time differences [19].

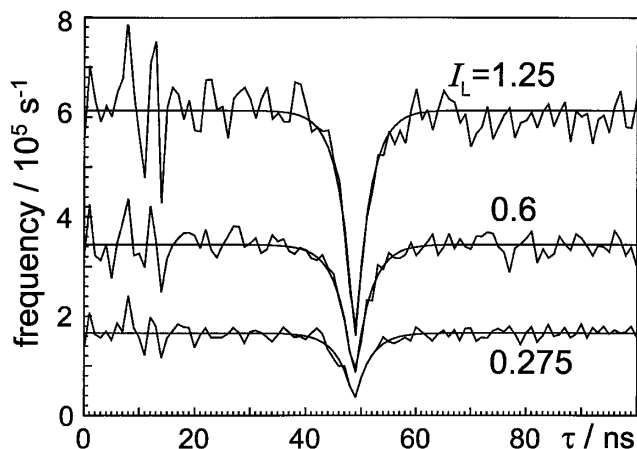


FIG. 1. Histograms of interphoton times measured for molecule M1 at several laser intensities  $I_L$  in  $\text{MW}/\text{cm}^2$  as indicated. The full lines represent fits to an exponential law.

To probe fluctuations on longer time scales ( $> t_{\text{dead}}$ ), the evolution of the photon rate is recorded as a time trace of photon numbers within a finite time bin from which  $g^{(2)}$  can be calculated using standard techniques [8,17].

To extract the short time scale information from our data, interphoton times were determined between a first photon recorded in one channel and the consecutive photon detected in the other channel. To exclude any influence from the SPAD dead time, only those pairs were included in the analysis for which both photodiodes were ready for detection at the arrival time of the first photon (typically 90% of all photons). Histograms of interphoton times for molecule M1 are shown in Fig. 1. They show dips at the electronic delay time  $t_{\text{delay}} = 48$  ns which are due to photon antibunching in the fluorescence light emitted by the molecule. This effect arises because the molecule, after emission of a photon, is prepared in the ground state  $S_0$  and has to be excited again before a second photon can be emitted. Photon antibunching is a clear signature of a nonclassical radiation field. It has been reported for single particles under various conditions [2,4]. Here, we observe this effect for the first time at room temperature without having to accumulate signals of many individual molecules [9–11]. The dips follow an exponential law  $\exp(-\alpha|t - t_{\text{delay}}|)$ . Extrapolation to zero laser intensity  $I_L$  can be applied to determine the fluorescence decay rate  $\alpha \approx k_{21}$ ,  $I_L \rightarrow 0$ .

To extract the longer time scale information from the stream of photons, the recorded arrival times of both channels were merged into bins of  $0.5 \mu\text{s}$  length in order to create a fluorescence time trace. From this time trace  $g^{(2)}(\tau) \approx 1 + C e^{-\beta\tau}$  was calculated (see Fig. 2). It shows photon bunching behavior due to intersystem crossing [17]. Photon bunching can be characterized by a decay rate  $\beta$  associated with the triplet relaxation rate  $k_{31}$  and a contrast  $C$ . We note that  $\beta$  increases strongly with the laser intensity while the contrast varies only weakly (as discussed below).

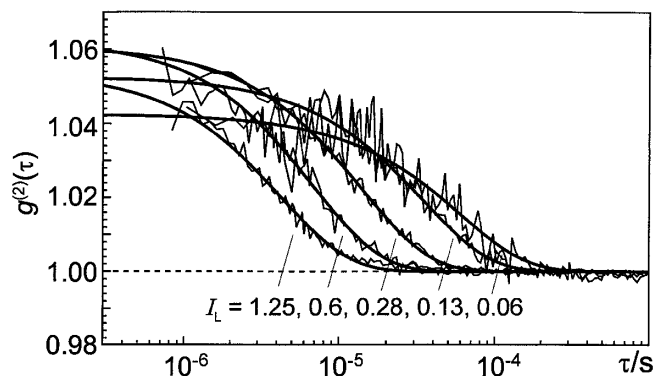


FIG. 2.  $g^{(2)}(\tau)$  obtained for molecule M1. The wiggly lines are the experimental data for several laser intensities in  $\text{MW}/\text{cm}^2$  as indicated. The smooth lines are fits to an exponential law.

For a more elegant analysis that covers all time scales, the two pieces of information from short start-stop time histograms and long time autocorrelation functions should be combined. This can be achieved using a method that was discussed by Reynaud [19]. We have adapted this method to the case of single-molecule fluorescence including background contributions. The method is based on two conjugated quantities denoted by  $K$  and  $J$ , where  $K(\tau)$  is the probability density that the next photon is recorded at time  $\tau$  provided that there was a photon at  $\tau = 0$ .  $K$  is identical to the histograms of interphoton times recorded in our experiment.  $J(\tau)$  is the number density of photons at time  $\tau$  provided that there was a photon at  $\tau = 0$ , thus

$$\bar{J}(\tau) = \langle I(t)I(t + \tau) \rangle. \quad (2)$$

From Eqs. (1) and (2) the relation  $J = \bar{J}g^{(2)}$  is evident. In the presence of background we write for the average photon rate

$$\bar{I} = \bar{I}_m + \bar{I}_b, \quad (3)$$

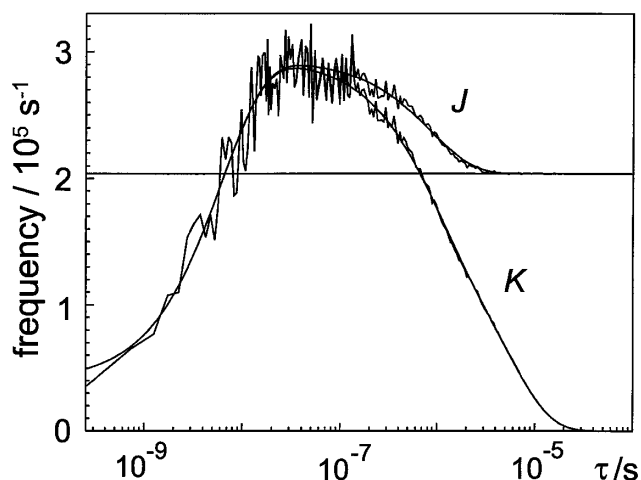


FIG. 3. Histograms  $K$  and  $J$ . The wiggly  $K$  is the normalized histogram of the experimental interphoton times determined for molecule M2 at an excitation intensity of  $450 \text{ kW}/\text{cm}^2$ . The wiggly  $J$  was calculated using FFT. The smooth  $J$  is a fit and the smooth  $K$  is the corresponding prediction.

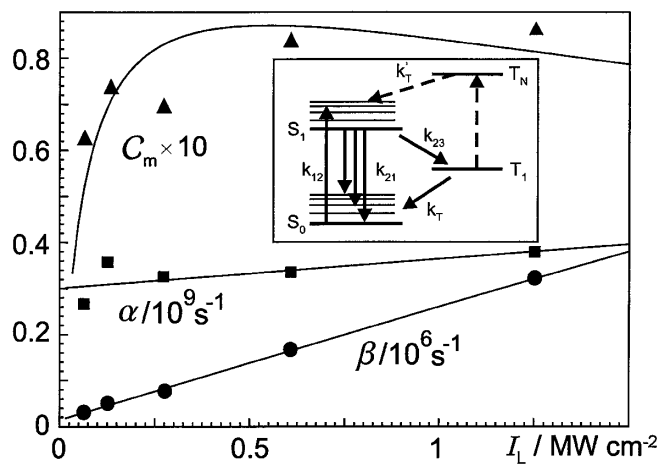


FIG. 4. Rates  $\alpha$  and  $\beta$  and contrast  $C_m$  as a function of the excitation intensity  $I_L$ . Symbols denote the values obtained from fits to the experimental data of molecule M1. The full lines are a fit to the model. Inset: Scheme of the relevant energy levels and transitions.

where the indices  $m$  and  $b$  refer to molecule and background, respectively. Assuming a Poissonian process for the background, one has

$$\bar{I}J(\tau) = \bar{I}_m J_m(\tau) + 2\bar{I}_m \bar{I}_b + \bar{I}_b^2. \quad (4)$$

The conjugated distributions  $J$  and  $K$  are related to each other by [19]

$$\tilde{J} \approx \tilde{K}/(1 - \tilde{K}), \quad (5)$$

where the tilde indicates Laplace transforms. Equation (5) is approximate because two qualitatively different processes, emission of a single quantum system and Poissonian background, are treated on an equal footing. However, thorough analysis has shown that for our data ( $\bar{I}_b \leq 0.2\bar{I}$ ) Eq. (5) is fulfilled with very good accuracy.

To determine  $J$  from recorded data sets, we first extracted the discrete interphoton times as described above, corrected for electronic delays, and built up  $K$  histograms with 0.5 ns bins. From the  $K$  histograms  $J$  was calculated according to Eq. (5). Laplace transforms are clearly not appropriate for the transformation of data stored as histograms. We therefore used an approximative algorithm based on fast Fourier transform (FFT), which allows for the determination of  $J$  from  $K$  over a time range of 6–7 orders of magnitude. An example of such a calculation is shown in Fig. 3 for molecule M2. As expected,  $K$  and  $J$  are indistinguishable for short times [19]. Deviations start

to become apparent for times  $>20$  ns. In particular, photon antibunching at short and photon bunching behavior at longer times are clearly visualized for a single molecule in a single plot [18].

The photon rate  $I_m(t)$  results from the spontaneous emission from  $S_1$  into the vibrational progression of  $S_0$  so that  $J_m(\tau) = \zeta k_r \rho_{22}(\tau)$ ,  $\rho_{22}(0) = 0$ , where  $k_r$  is the radiative fluorescence rate,  $\rho_{22}$  is the population of  $S_1$ , and  $\zeta$  is the overall detection efficiency. At ambient temperature and nonresonant excitation, a system of rate equations is appropriate to describe the population of the molecular levels  $S_0$ ,  $S_1$ , and  $T_1$ , as schematically shown in the inset in Fig. 4. Here,  $k_{12} = \sigma I_L$  denotes the  $S_0 \rightarrow S_1$  pump rate depending on the absorption cross section  $\sigma$  and the laser intensity  $I_L$ ,  $k_{21} = k_r + k_{nr}$  is the  $S_1 \rightarrow S_0$  relaxation rate with  $k_{nr}$  the nonradiative component,  $k_{23}$  is the intersystem crossing rate, and  $k_{31}$  is the triplet relaxation rate. The rate equations can be solved analytically, resulting in

$$J_m = a(1 - e^{-\alpha t}) - b(1 - e^{-\beta t}). \quad (6)$$

Identifying  $\alpha$  with the fast and  $\beta$  with the slow decay rates, the first and second terms relate to photon antibunching and bunching, respectively. The contrast resulting only from photon bunching is  $C_m = b/(a - b)$ . The overall contrast with background included is  $C = C_m(\bar{I}_m/\bar{I})^2$ . The background was less than 20% of the signal in all cases. For the description of  $J$ , a set of five parameters,  $\alpha$ ,  $\beta$ ,  $C_m$ ,  $\bar{I}_m$ , and  $\bar{I}_b$ , has to be fitted according to Eqs. (4) and (6). Such a fit is shown in Fig. 3 for molecule M2. From the fitted parameters  $K$  was calculated analytically from straightforward Laplace transforms using Eq. (5). The result is also shown in Fig. 3. The theoretical curves match the observations up to the experimental resolution.

The above parameter set was determined for several molecules and for several laser intensities below saturation. For molecule M1,  $\alpha$ ,  $\beta$ , and  $C_m$  are displayed in Fig. 4.  $\alpha$  increases slowly with  $I_L$  as expected.  $\beta$ , on the contrary, depends strongly on  $I_L$  with a very small offset, while  $C_m$  does hardly change with increasing  $I_L$ , in agreement with the data in Fig. 2. For slow intersystem crossing the following approximate expressions apply:  $\alpha \approx \sigma I_L + k_{21}$ ,  $\beta \approx k_{31} + \sigma I_L k_{23}/(\sigma I_L + k_{23})$ , and  $C_m \approx \sigma I_L k_{23}/[k_{31}(\sigma I_L + k_{23})]$ . Inserting the expression for  $C_m$  into that of  $\beta$  one has  $\beta \approx k_{31}(1 + C_m)$ . This equation is incompatible with the observations, unless a variation of  $k_{31}$  with laser intensity is supposed. We therefore introduced the linear dependence  $k_{31} = k_T + k'_{31} I_L$

TABLE I. Transition rates of molecules M1–M3. For  $k_{31}$  the ranges of observed values are given.  $k_T$  fixed for M2.

Molecule	$\sigma$ $10^{-17} \text{ cm}^2$	$k_{21}$ $10^8 \text{ s}^{-1}$	$k_{23}$ $10^5 \text{ s}^{-1}$	$k_T$ $10^3 \text{ s}^{-1}$	$k_{31}$ $10^5 \text{ s}^{-1}$
M1	1.4	3.0	1.2	14.0	2–30
M2	7.5	1.2	23.0	3.5	2–30
M3	2.5	1.7	4.4	3.2	1–5

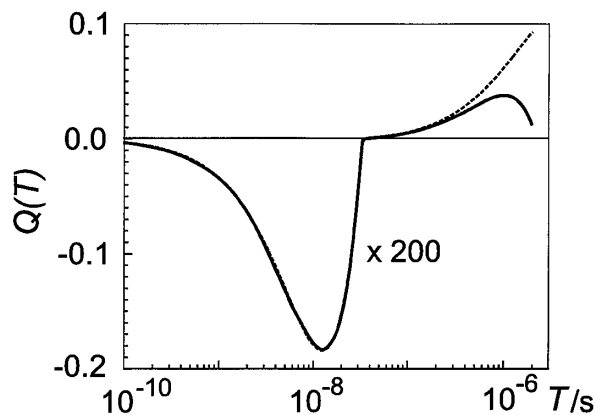


FIG. 5. Normalized second factorial moment  $Q(T)$ . Full line: experimental data of molecule M2. Dashed line: prediction according to Eqs. (4) and (7). For visibility, the negative values are enlarged by a factor of 200.

with  $k_T$  and  $k'_{31}$  as two independent parameters. The parameters  $\sigma$ ,  $k_{21}$ ,  $k_{23}$ ,  $k_T$ , and  $k'_{31}$  were simultaneously fitted to the set of experimentally determined  $\alpha$ ,  $\beta$ , and  $C_m$  values. Results of the fit are shown in Fig. 4 for molecule M1. The data of M1 and two further molecules are collected in Table I. The parameters change from molecule to molecule. The fluorescence decay rates are typically  $k_{21} = 2 \times 10^8 \text{ s}^{-1}$ . The  $k_{23}$  values are by 2–3 orders of magnitude larger than  $k_{23} = 540 \text{ s}^{-1}$  at 1.8 K [20]. The fitted  $k_T$  are compatible with the low-temperature value of triplet relaxation  $k_T \approx 3 \times 10^3 \text{ s}^{-1}$  at 1.8 K [20], while typical values of  $k_{31}$  are larger than  $k_T$  by 2–3 orders of magnitude. We interpret the dependence of  $k_{31}$  on the laser intensity as resulting from pumping higher triplet states [21] from the lowest triplet state associated with an accelerated reverse intersystem crossing as indicated by  $k'_T$  in the inset in Fig. 4. We speculate that the remarkable photostability of terylene at ambient conditions has to do with this mechanism.

Photon antibunching and bunching is usually connected with sub- and super-Poissonian statistics in the probability distribution of photon numbers detected in a given time interval. The occurrence of sub-Poissonian statistics is a second criterion of a nonclassical radiation field. For its characterization the normalized second factorial moment is considered,  $Q(T) = (\langle(\Delta n)^2\rangle - \langle n \rangle^2) / \langle n \rangle$ , where  $n$  is the number of photons within a time interval  $T$  and  $(\Delta n)^2$  is the variance. Negative, zero, and positive  $Q$  values indicate sub-, regular, and super-Poissonian behavior, respectively.  $Q$  is related to  $J$  by [22]

$$Q(T) = \frac{2}{T} \int_0^T dt' \int_0^{t'} J(t'') dt'' - \bar{I}T. \quad (7)$$

For sufficiently short times,  $J$  can be approximated by  $K$ , so that  $Q(T)$  can be directly calculated from the recorded interphoton time histogram. The result is shown in Fig. 5. Because of the cumulative integrals in Eq. (7), the scatter of the data is completely smoothed out. The agree-

ment with predictions calculated from Eqs (4) and (7) is excellent for short times where sub-Poissonian behavior is clearly observed. At longer times, deviations appear when also  $K$  deviates from  $J$ , as is visible in Fig. 3.

We are grateful to Dr. T. Plakhotnik for bringing to our attention the issue of sub-Poissonian photon statistics. We acknowledge stimulating discussions with E. Donley, T. Nonn, M. Prummer, Dr. A. Renn, B. Sick, and W. Trabesinger. This work was supported by the Swiss National Science Foundation and by the ETH-Zürich.

\*Electronic address: hecht@phys.chem.ethz.ch

- [1] H. J. Kimble, M. Dagenais, and L. Mandel, Phys. Rev. Lett. **39**, 691 (1977).
- [2] F. Diedrich and H. Walther, Phys. Rev. Lett. **58**, 203 (1987).
- [3] W.E. Moerner and L. Kador, Phys. Rev. Lett. **62**, 2535 (1989); M. Orrit and J. Bernard, Phys. Rev. Lett. **65**, 2716 (1990); T. Plakhotnik, E. Donley, and U.P. Wild, Annu. Rev. Phys. Chem. **48**, 181 (1997); W.E. Moerner and M. Orrit, Science **283**, 1670 (1999).
- [4] T. Basché, W.E. Moerner, M. Orrit, and H. Talon, Phys. Rev. Lett. **69**, 1516 (1992).
- [5] P. Tamarat, B. Lounis, J. Bernard, M. Orrit, S. Kummer, R. Kettner, S. Mais, and T. Basché, Phys. Rev. Lett. **75**, 1514 (1995).
- [6] B. Lounis, F. Jelezko, and M. Orrit, Phys. Rev. Lett. **78**, 3673 (1997).
- [7] C. Brunel, B. Lounis, P. Tamarat, and M. Orrit, Phys. Rev. Lett. **81**, 2679 (1998).
- [8] X.S. Xie and J.K. Trautman, Annu. Rev. Phys. Chem. **49**, 441 (1998).
- [9] F. De Martini, G. Di Giuseppe, and M. Marrocco, Phys. Rev. Lett. **76**, 900 (1996).
- [10] M. Wu, P.M. Goodwin, W.P. Ambrose, and R.A. Keller, J. Phys. Chem. **100**, 17406 (1996).
- [11] W.P. Ambrose, P.M. Goodwin, J. Enderlein, D.J. Semin, J.C. Martin, and R.A. Keller, Chem. Phys. Lett. **269**, 365 (1997).
- [12] F. De Martini, G. Innocenti, G.R. Jacobovitz, and P. Mat-aloni, Phys. Rev. Lett. **59**, 2955 (1987).
- [13] D.J. Norris, M. Wuwate-Gonokami, and W.E. Moerner, Appl. Phys. Lett. **71**, 297 (1997).
- [14] L. Fleury, B. Sick, G. Zumofen, B. Hecht, and U.P. Wild, Mol. Phys. **95**, 1333 (1998).
- [15] S. Kummer, F. Kulzer, R. Kettner, T. Basché, C. Tietz, C. Glowatz, and C. Kryschi, J. Chem. Phys. **107**, 7673 (1997).
- [16] Guide Technology, Sunnyvale, CA 94086.
- [17] J. Bernard, L. Fleury, H. Talon, and M. Orrit, J. Chem. Phys. **98**, 850 (1993).
- [18] S. Kummer, S. Mais, and T. Basché, J. Phys. Chem. **99**, 17078 (1995).
- [19] S. Reynaud Ann. Phys. (Paris) **8**, 351 (1983).
- [20] A.C.J. Brouwer, E.J.J. Groenen, and J. Schmidt, Phys. Rev. Lett. **80**, 3944 (1998).
- [21] C. Eggeling, J. Widengren, R. Rigler, and C.A.M. Seidel, Anal. Chem. **70**, 2651 (1998).
- [22] R. Short and L. Mandel, Phys. Rev. Lett. **51**, 384 (1983).